The TeV-detected radio galaxy 3C 264: a science case in the perspective of CTA

Giulia Migliori (IRA)
B.Boccardi (MPIFR), P.Grandi (OAS), E.Torresi (OAS), F.Mertens (Kapteyn), V.Karamanavis, A.Angioni, C.Vignali (DIFA)

Boccardi et al., A&A 2019:arXiv:1905.06634

3C 264

INAF IRA

- FRI/LERG radio galaxy (D_L=94 Mpc) in Abell 1367 cluster;
- Head-tail kpc structure with extended radio, optical, X-ray jet (Lara+'97, Perlman+'10, Meyer+'15);
- Gamma-ray detected by Fermi (Γ=1.94±0.10, $F_{1\text{-}100GeV}$=(2.85 ± 0.40) × 10^{-10} phot s^{-1} cm^{-2});
- VHE candidate (Angioni+'17)=> MAGIC proposal (PI:Angioni)

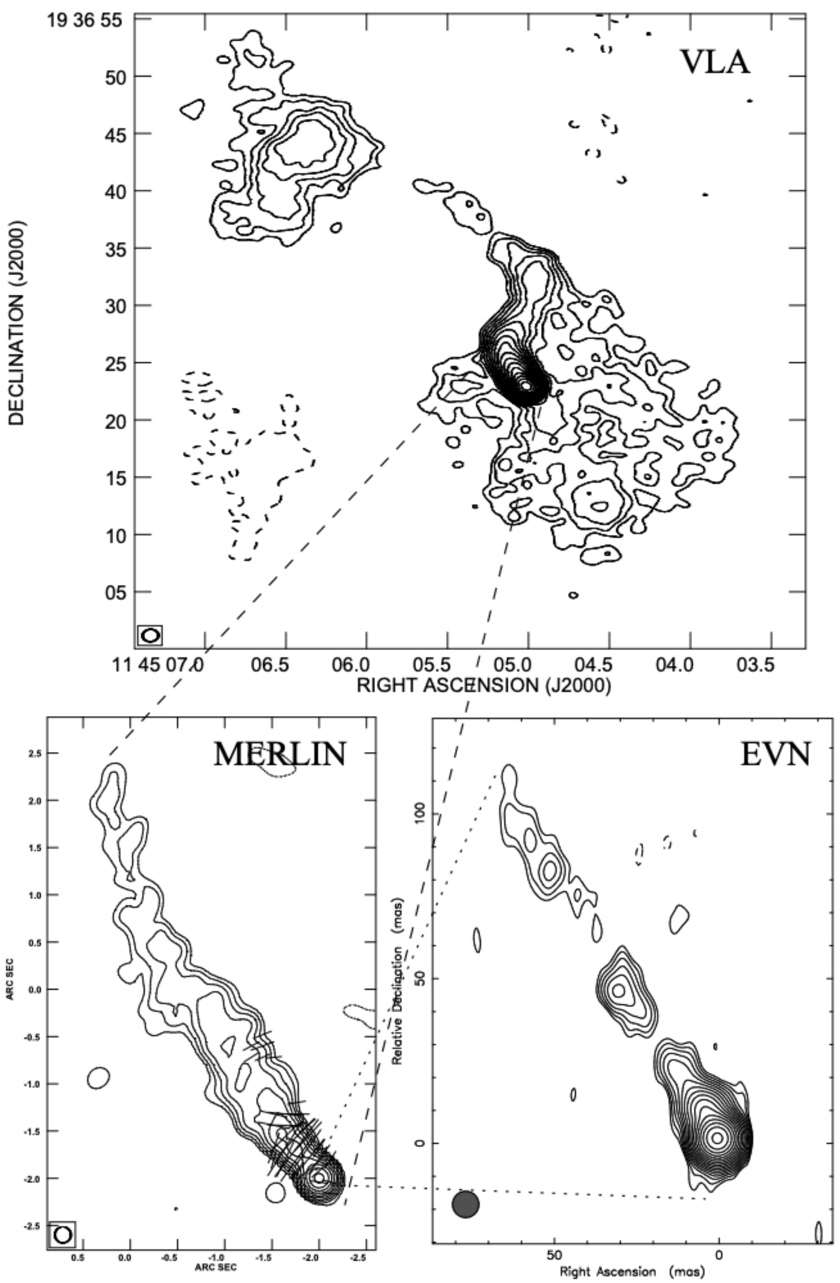

(Lara+'04)

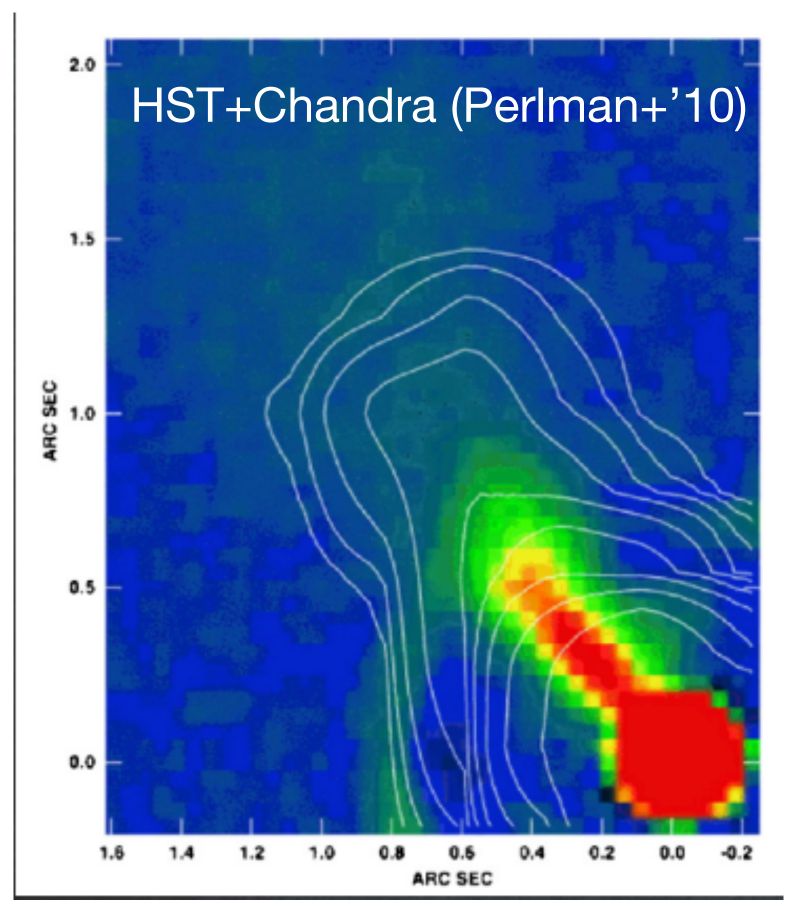

Optical jet: app. superluminal motion (Meyer+'15)

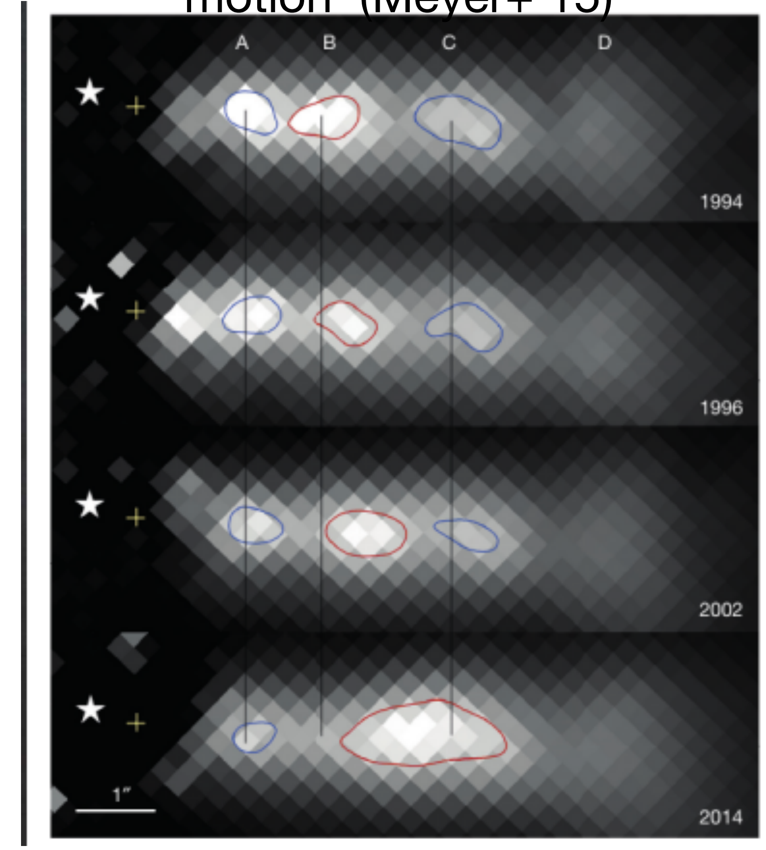

3C 264: VHE

VERITAS detection in 2018 (Archer+'18):

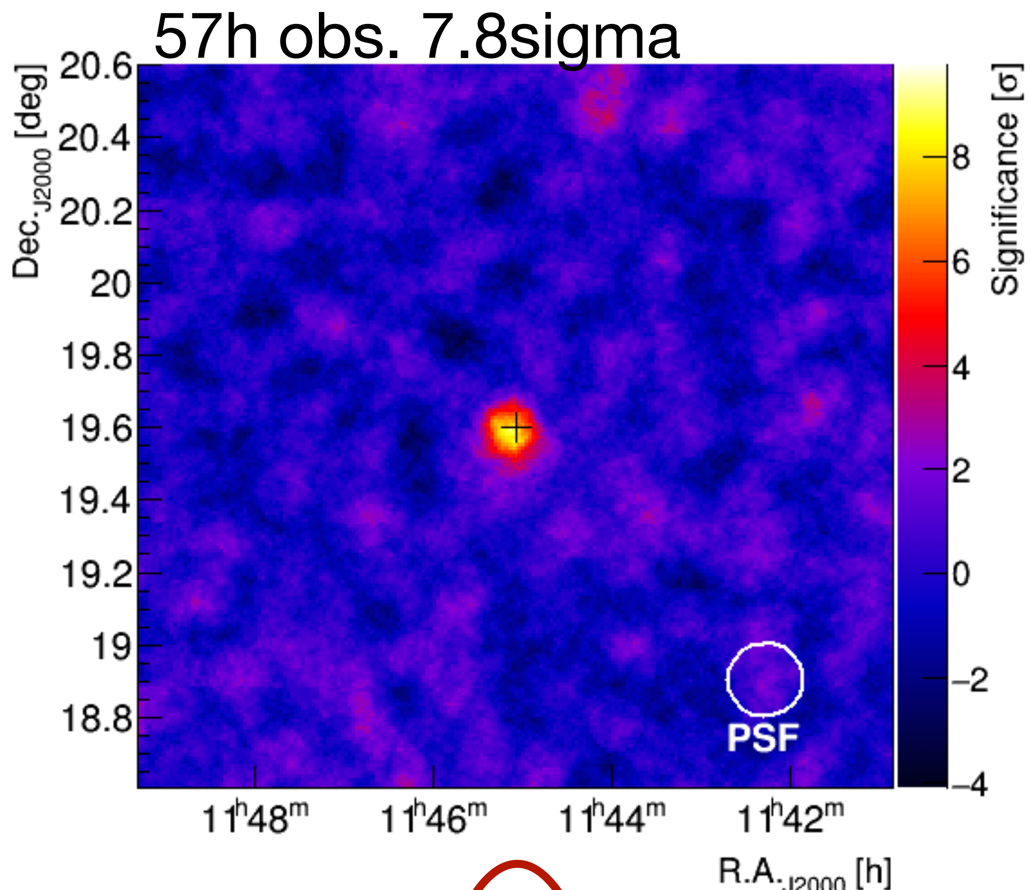

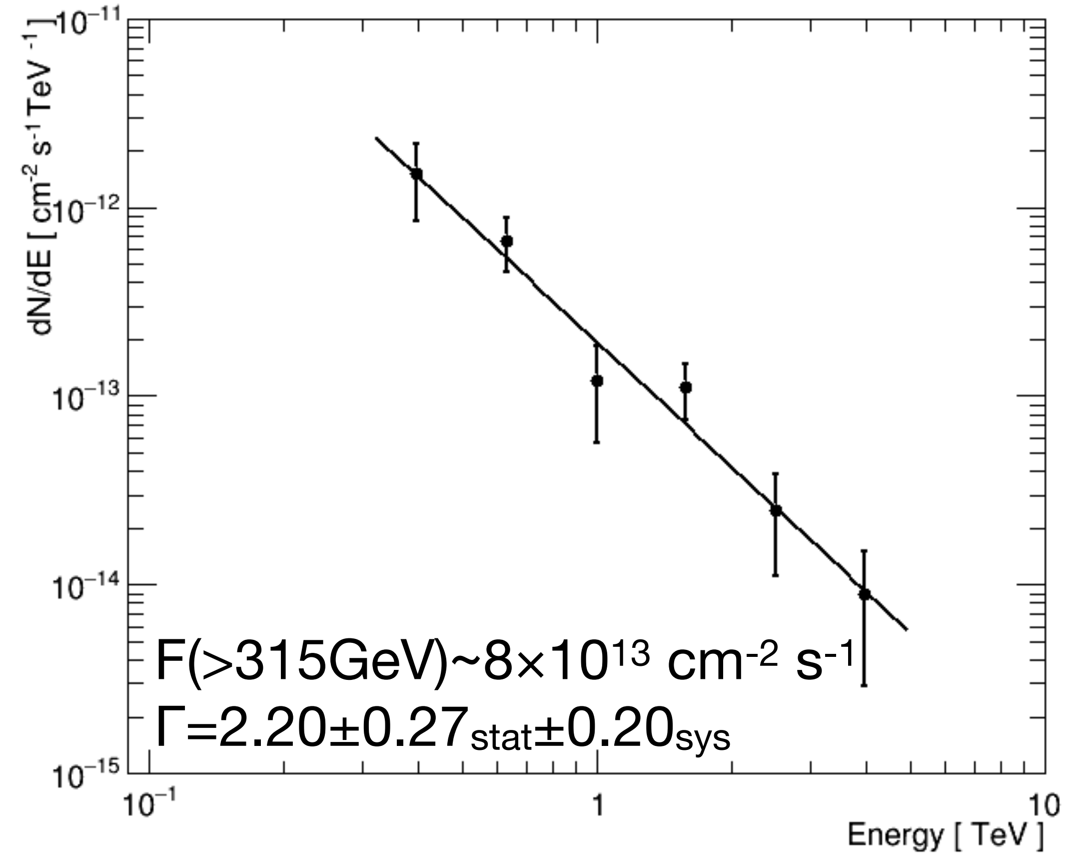

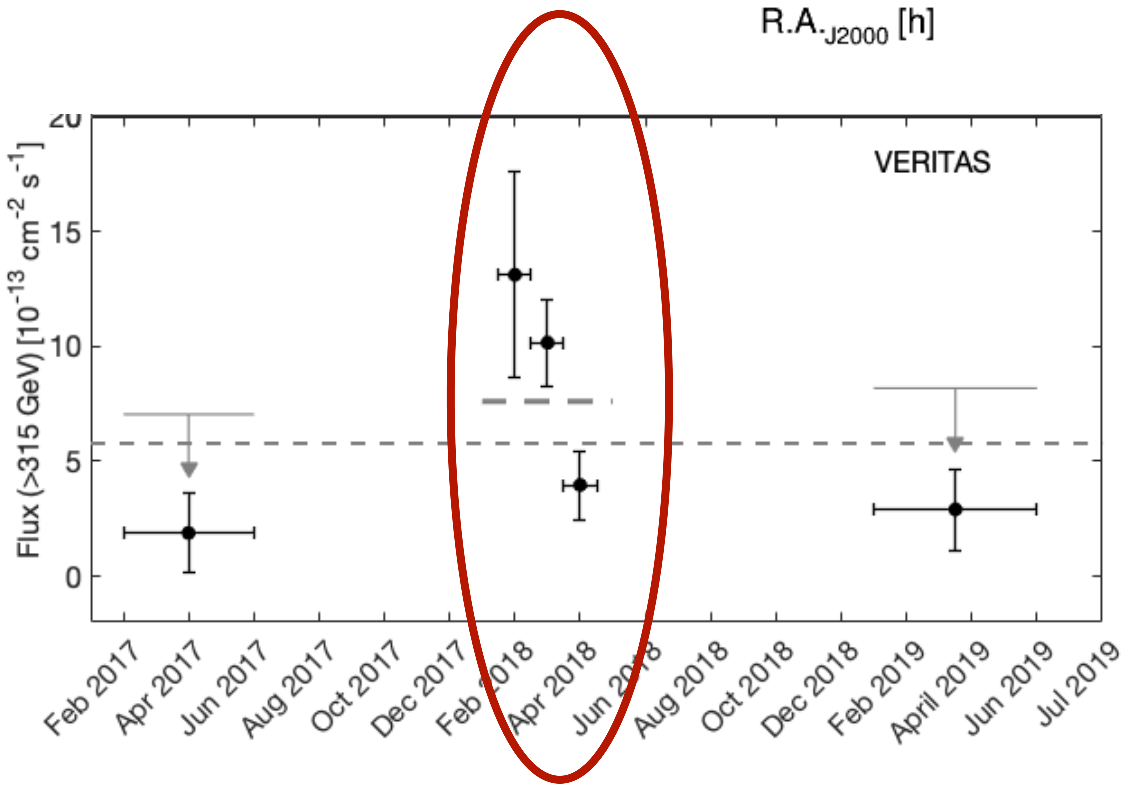

- Monthly variable VHE flux rather than strong flare;
- Fermi-LAT: hints of enhanced MeV-GeV emission

Low amplitude γ-ray variability

3C 264 jet: X-rays

INAF IRA

Year-to-month scale monitoring:

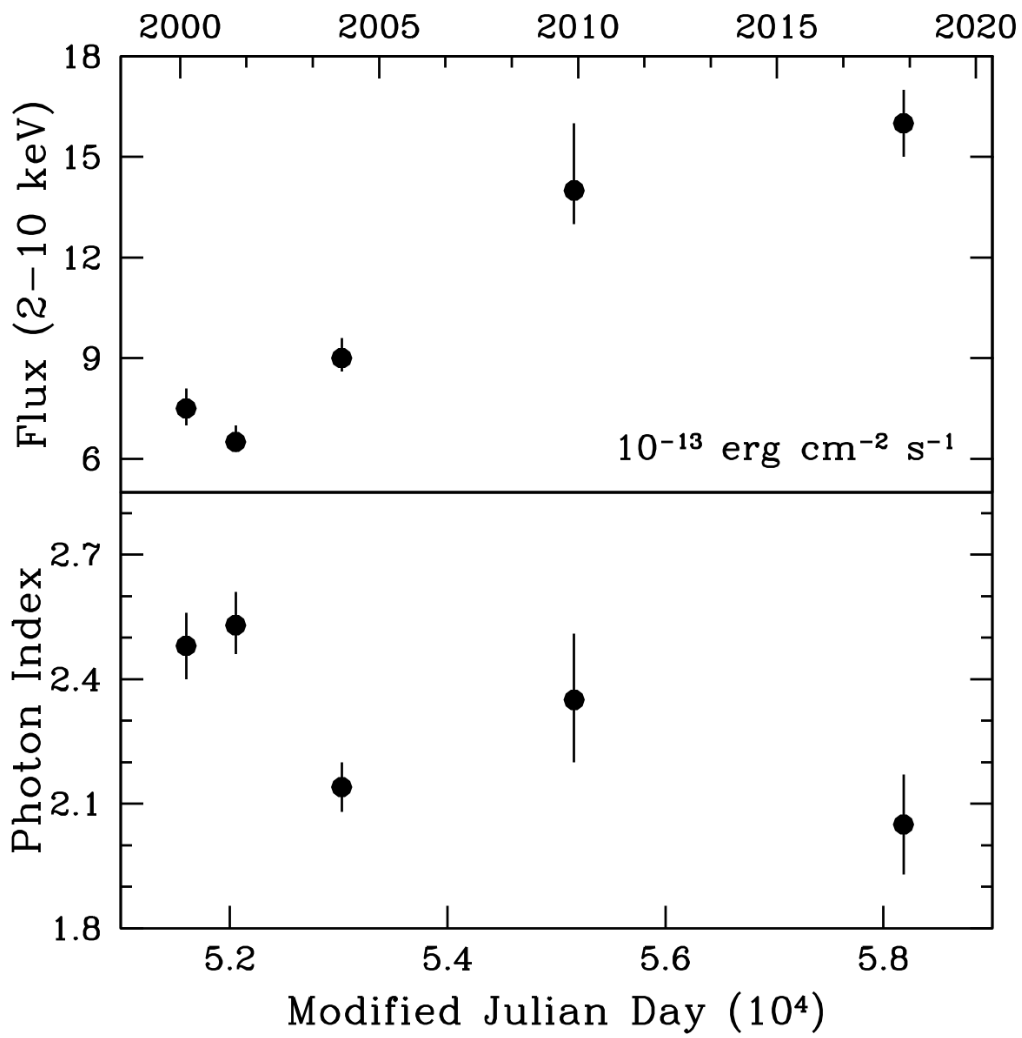

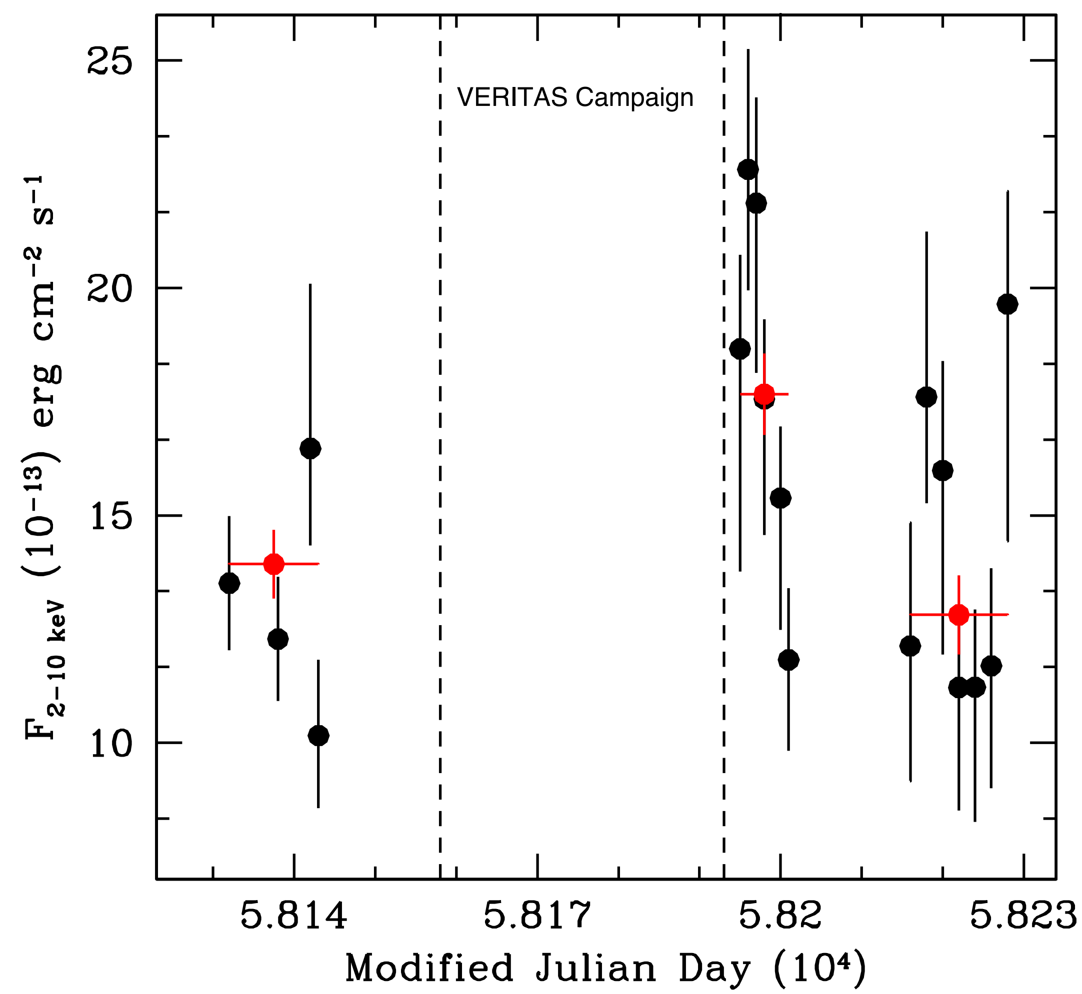

- Non-thermal core emission ($\Gamma_{X\text{-rays}}$=1.8-2.5, $L_{2\text{-}10keV}$=(8-30)×10^{41} erg s^{-1});
- Long term variability: ×3 flux increase from 2000 to 2018 + harder when brighter trend?
- Short term variability (<3days): high(er) state immediately after the VHE detection.

3C 264 jet: inner structure

INAF IRA

MOJAVE VLBA 15 GHz (Sept 2016 - Oct 2018)

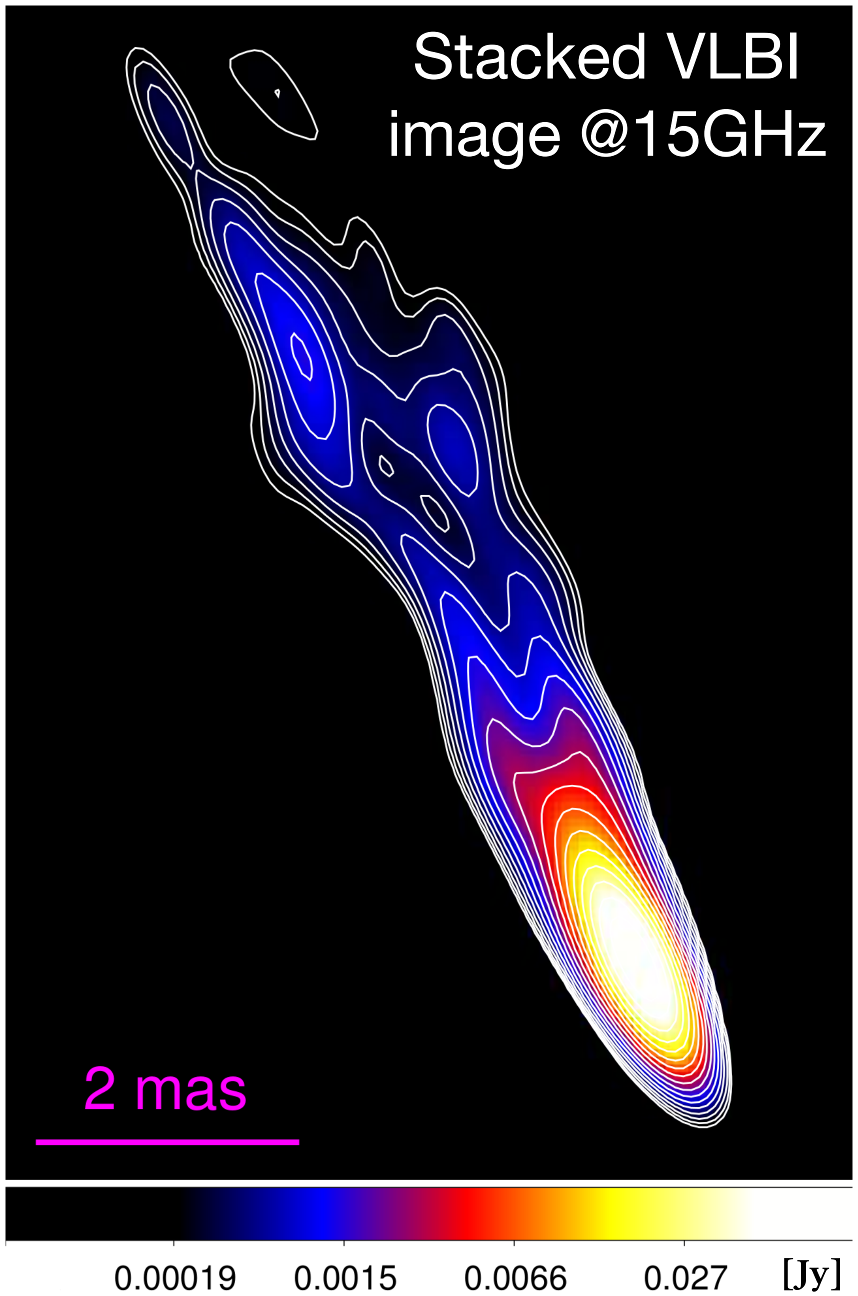

- Moderately variable radio core (+20% in 2018);
- Limb brightened structure at parsec scales + one knot;
- Analysis of the inner jet features via WISE code:

1. multiscale wavelet decomposition for each epoch

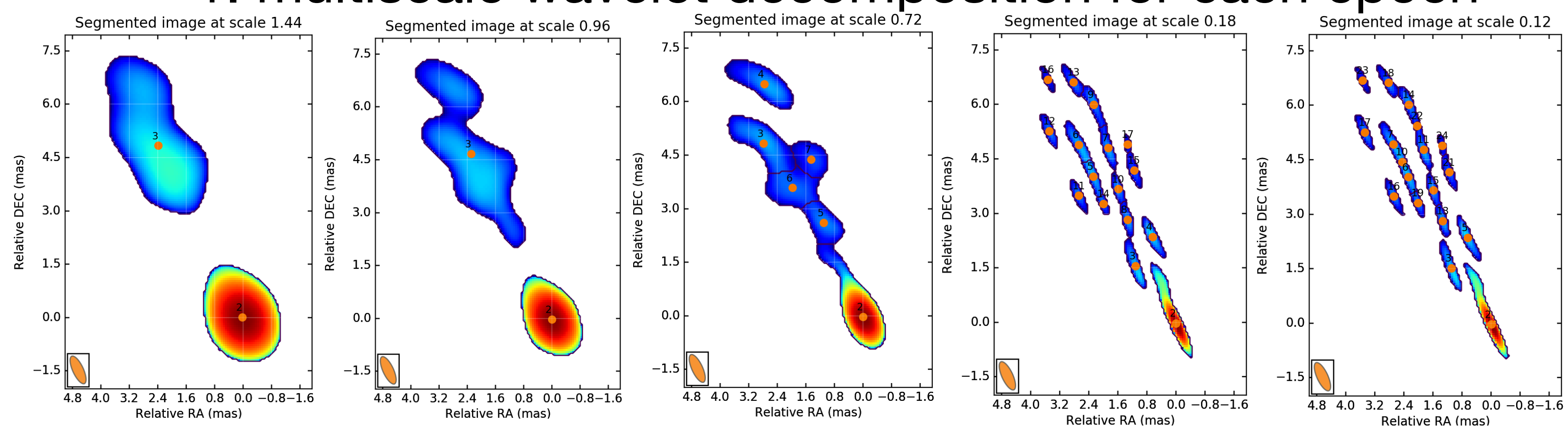

2. wavelet decomposition through the epochs (same scale)

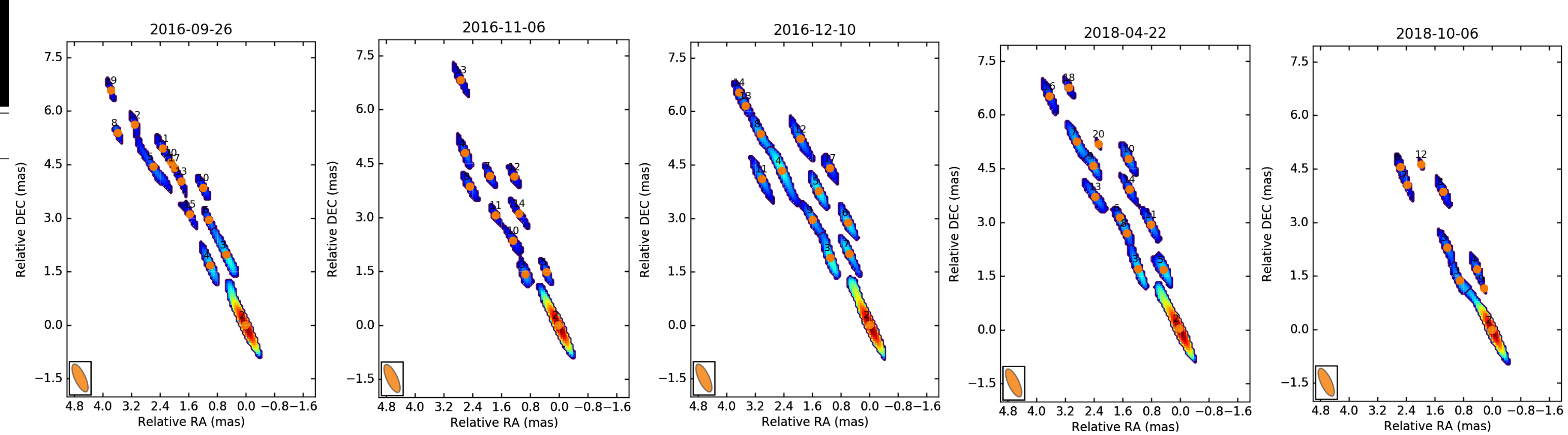

3C 264 jet: kinematics

INAF IRA

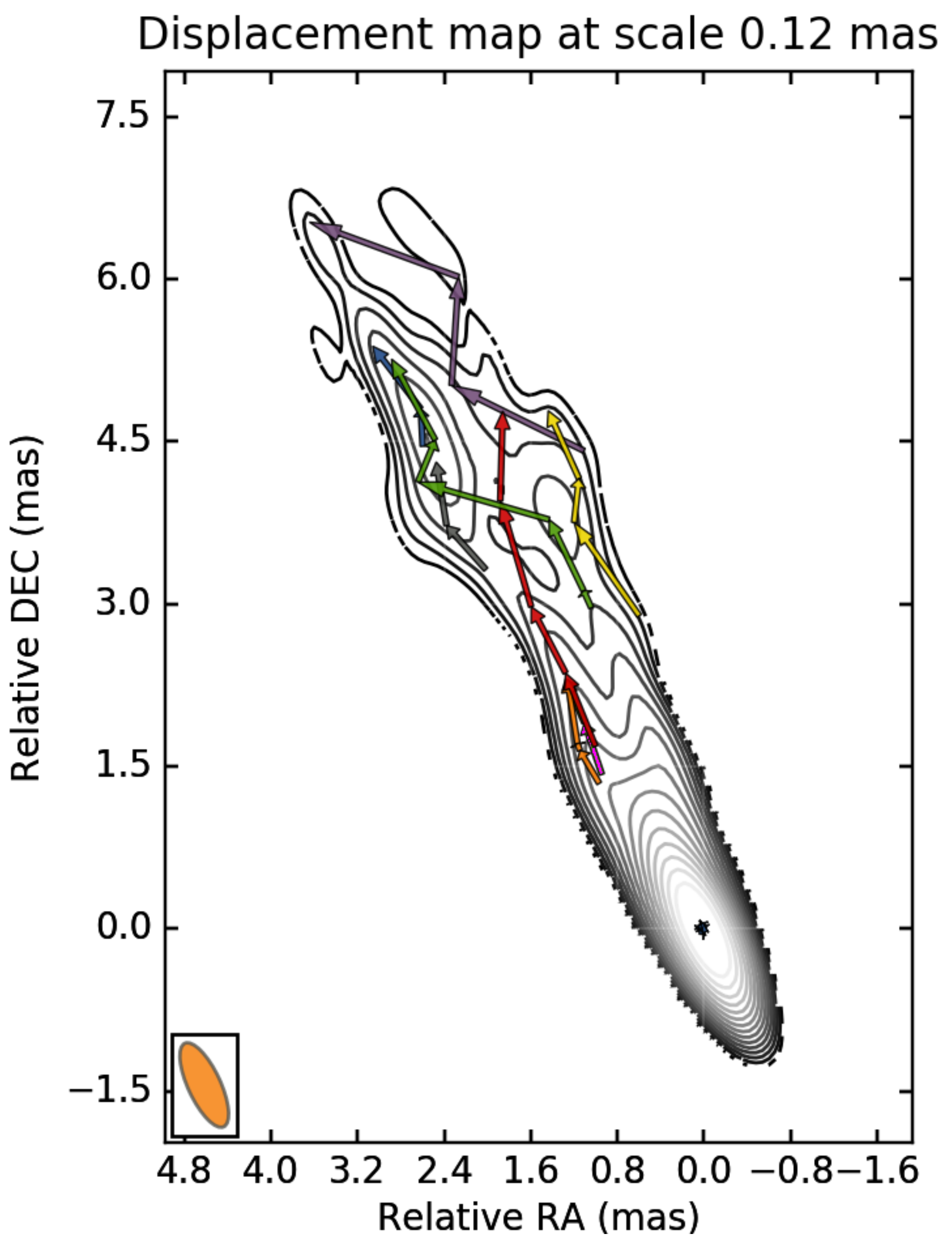

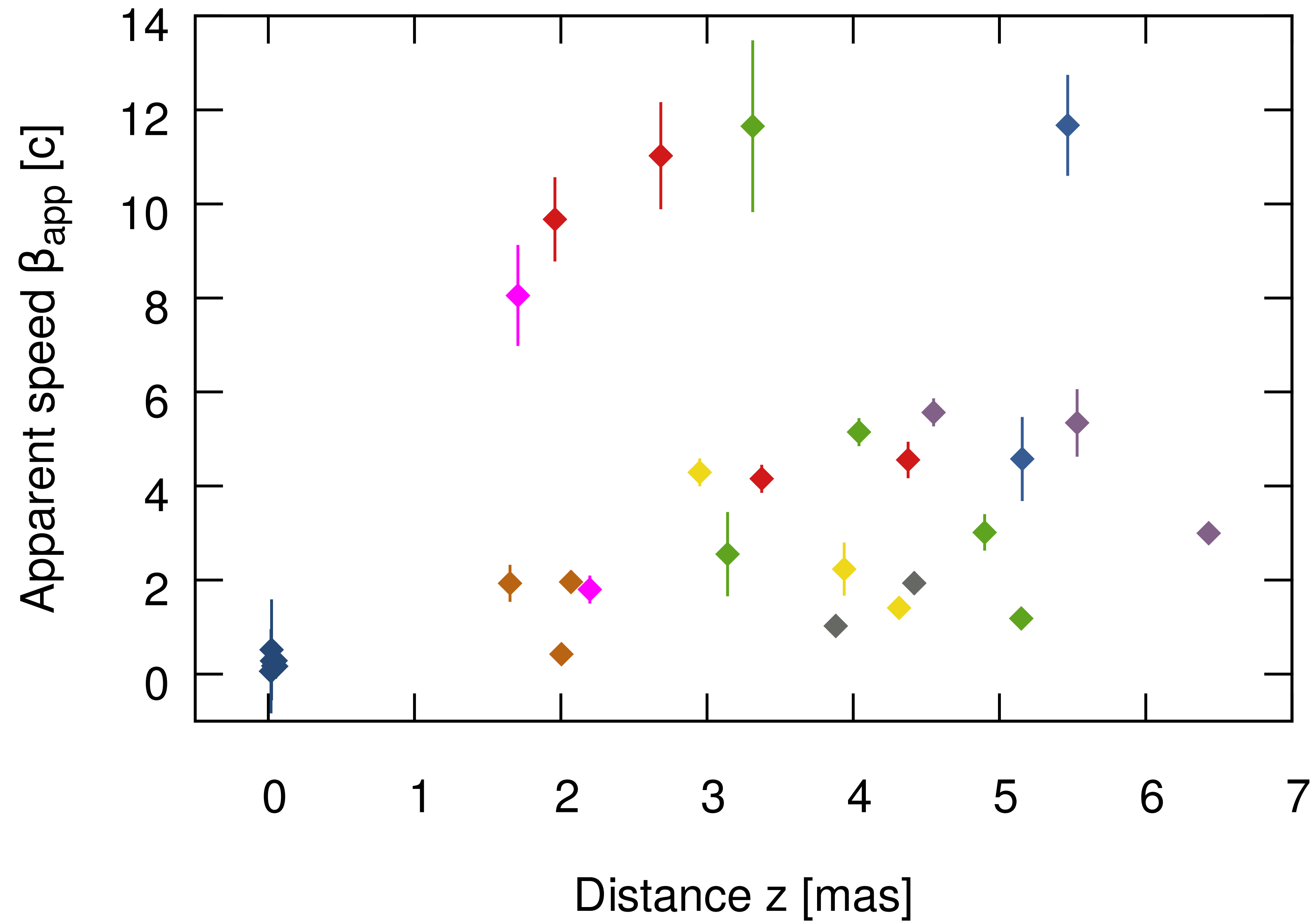

- Apparent bulk flow speed increases up to 11c:
  - constraints on the jet viewing angle ($\theta_{max} \lesssim 10°$) and bulk motions ($\Gamma_{bulk}$~5-15)
- Acceleration zone extends to 11 pc (~5×10^4 R_S).

3C 264 jet: collimation

INAF IRA

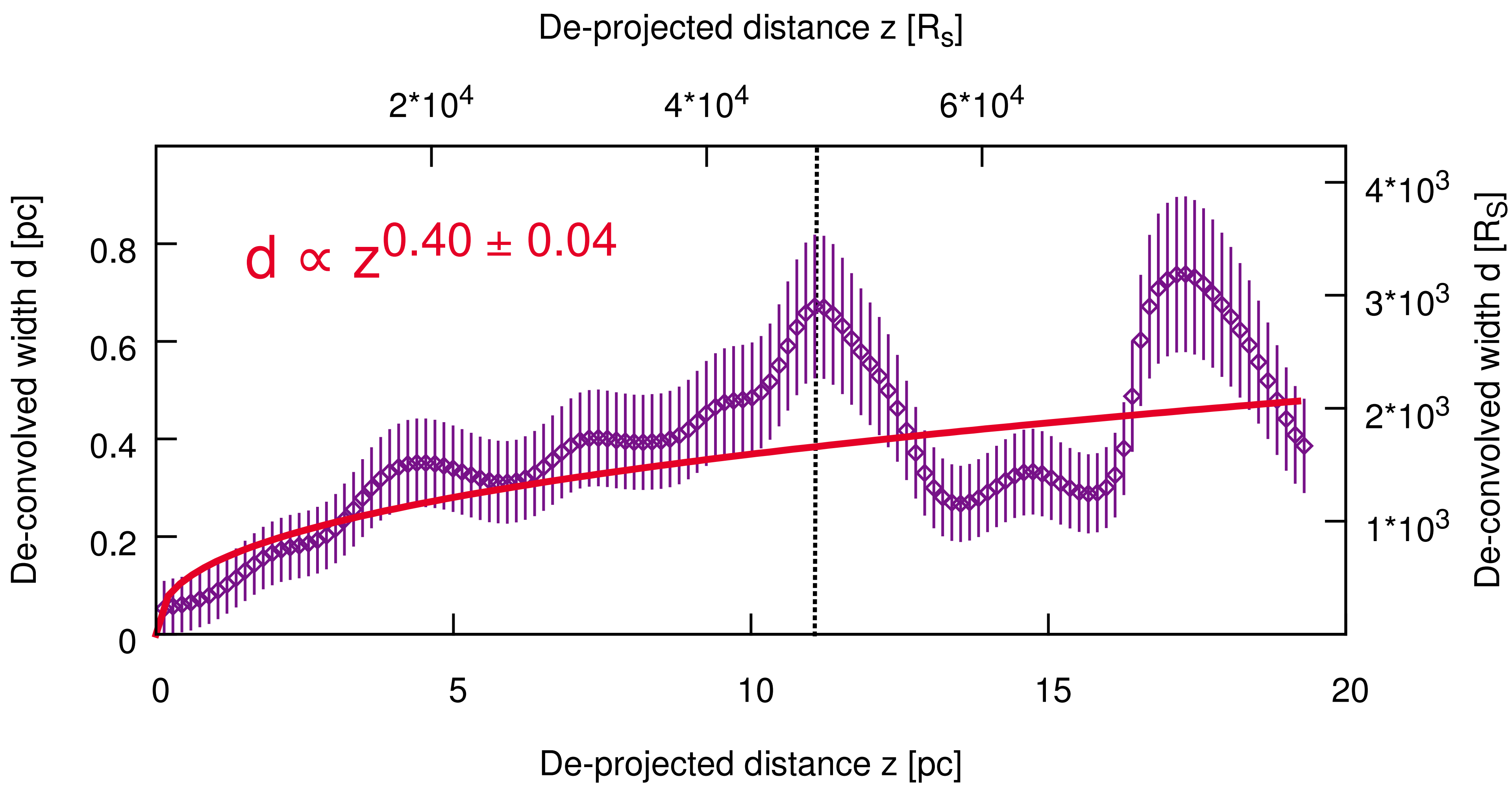

- The jet has a nearly parabolic shape on pc-scales;
- The recollimation starts at ~11pc distance;

collimation & acceleration take place over the same scales

3C 264 jet: SED

- Radio jet parameters between BL Lacs and FR I radio galaxies & double hump SED;
- No evidences of accretion features in the optical/UV band;
- Low amplitude gamma-ray & X-ray flux (and spectral?) variability.

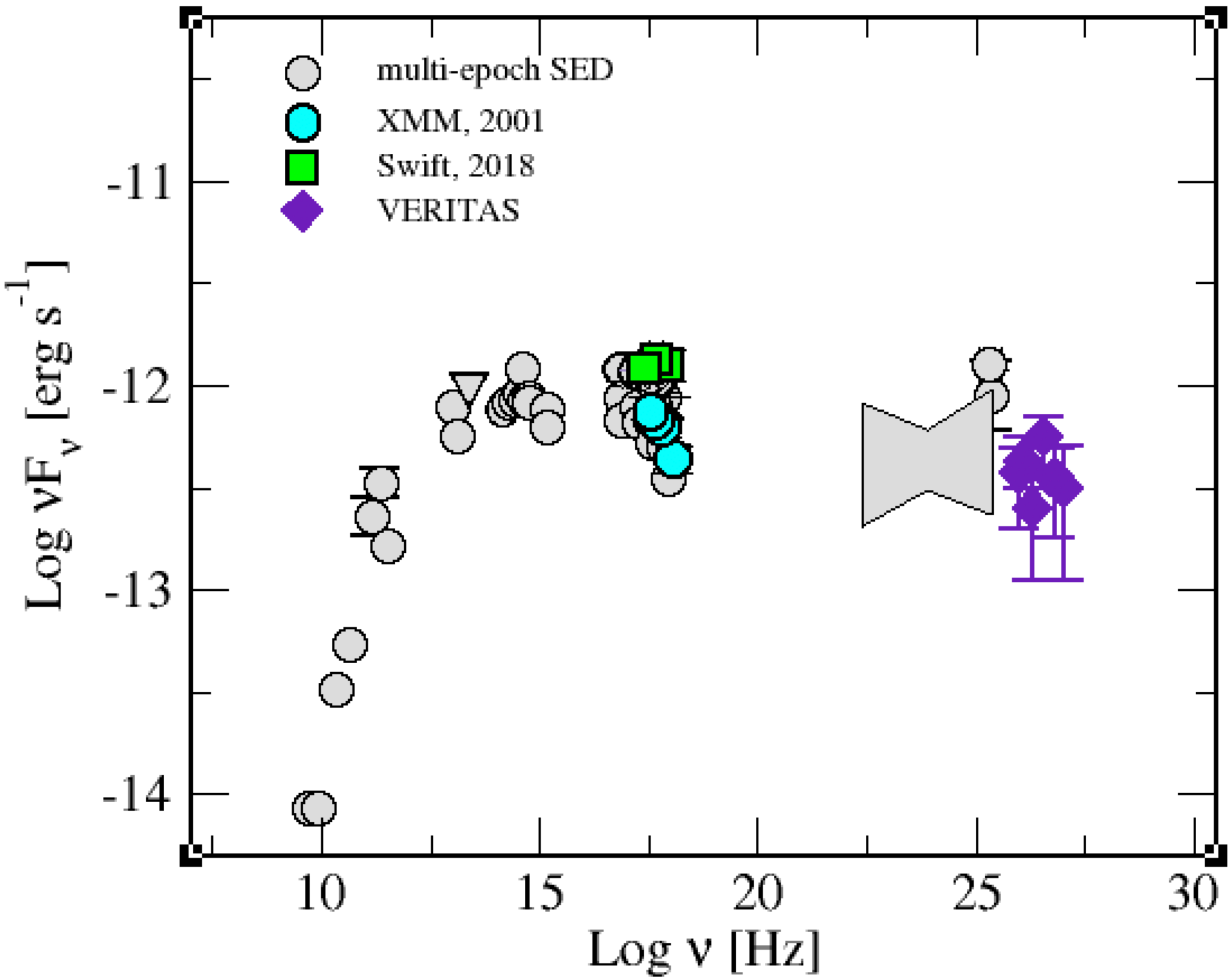

3C 264 jet: SED

Working hypothesis:

3C 264 switches between a low/soft state (LSS) vs high/hard state (HHS)

+

LSS is the "average" emission produced in a mildly relativistic region at the base of the acceleration zone (radio core)

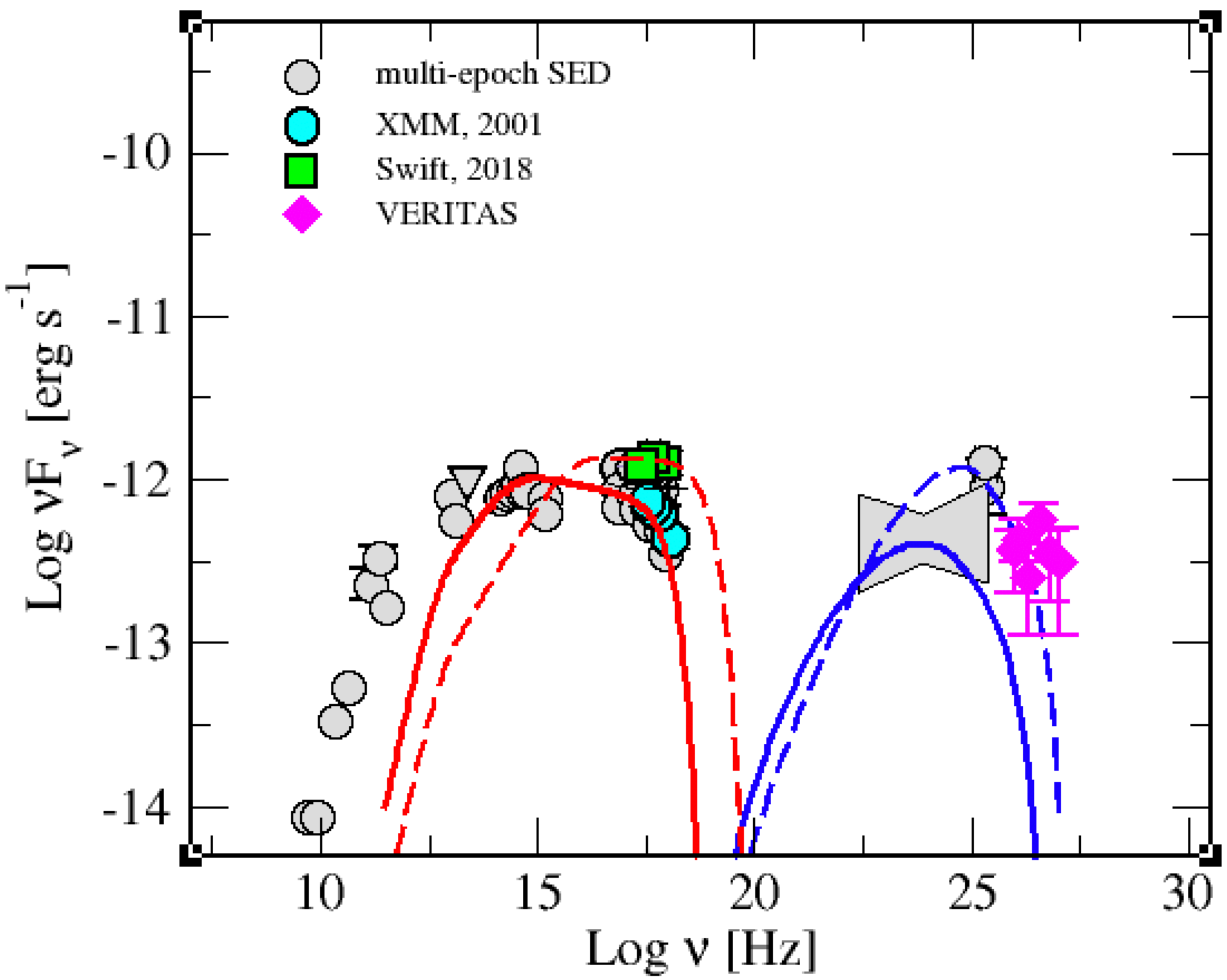

- **One zone model:** LSS and HHS produced by one blob located in the radio core

Need $U_e \gg U_B$ in contrast with theoretical predictions of the jet being magnetised in the launching region (same for TeV BL Lacs e.g. Tavecchio+'10)

3C 264 jet: SED

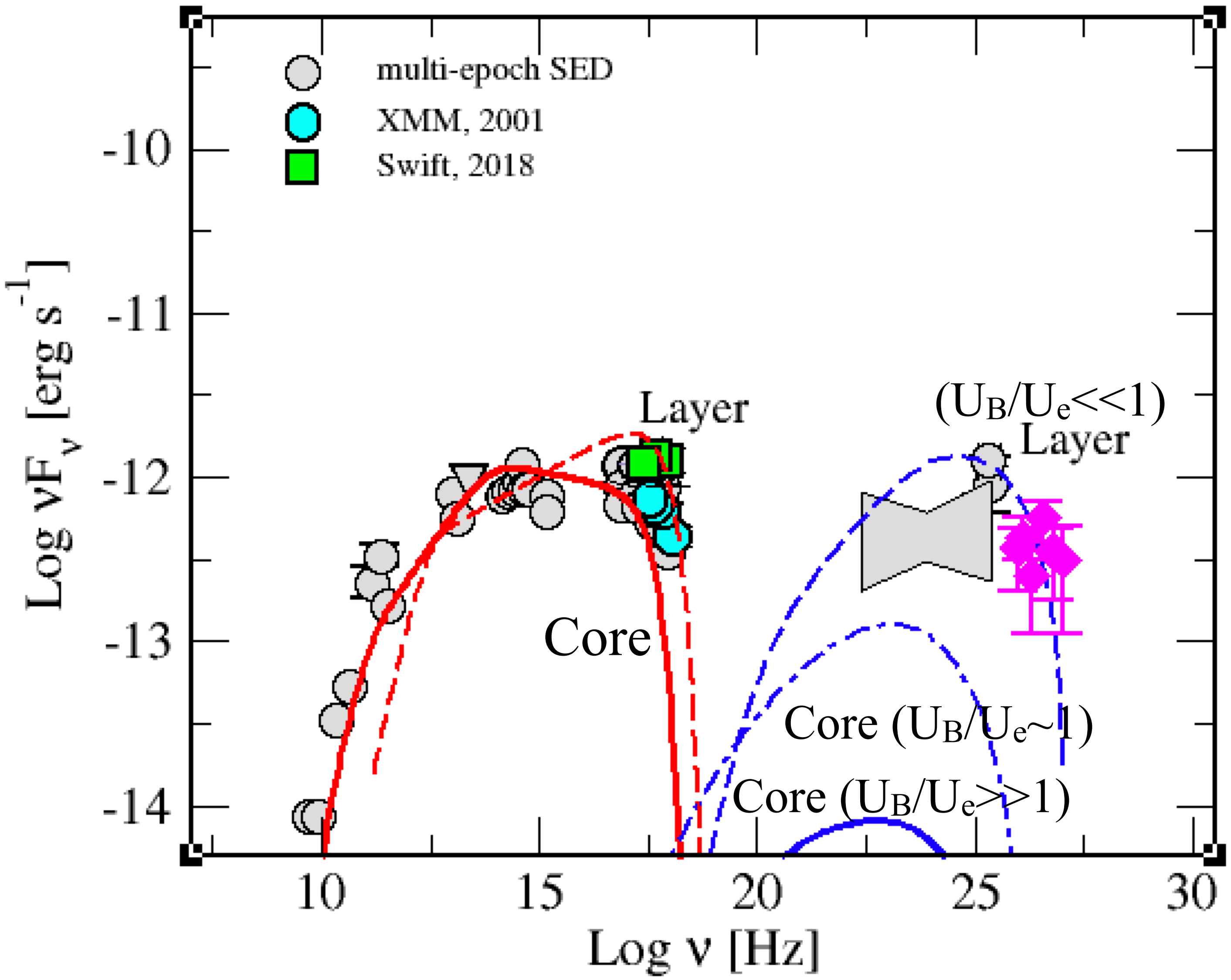

Multi-zone model:

- SLS in a Poynting flux dominated region of the core and HHS produced at the end of the acceleration region (particle dominated) by a blob with Γ_{bulk}~5-15;
- The observed variability due to changes of the Doppler factor/viewing angle (as proposed for CTA 102, Raiteri+'17)

Conclusions & future

INAF IRA

- VLBI observations probe the acceleration and collimation zones of the jets and provide key constraints to the particle acceleration & radiative models for the HE/VHE emission;

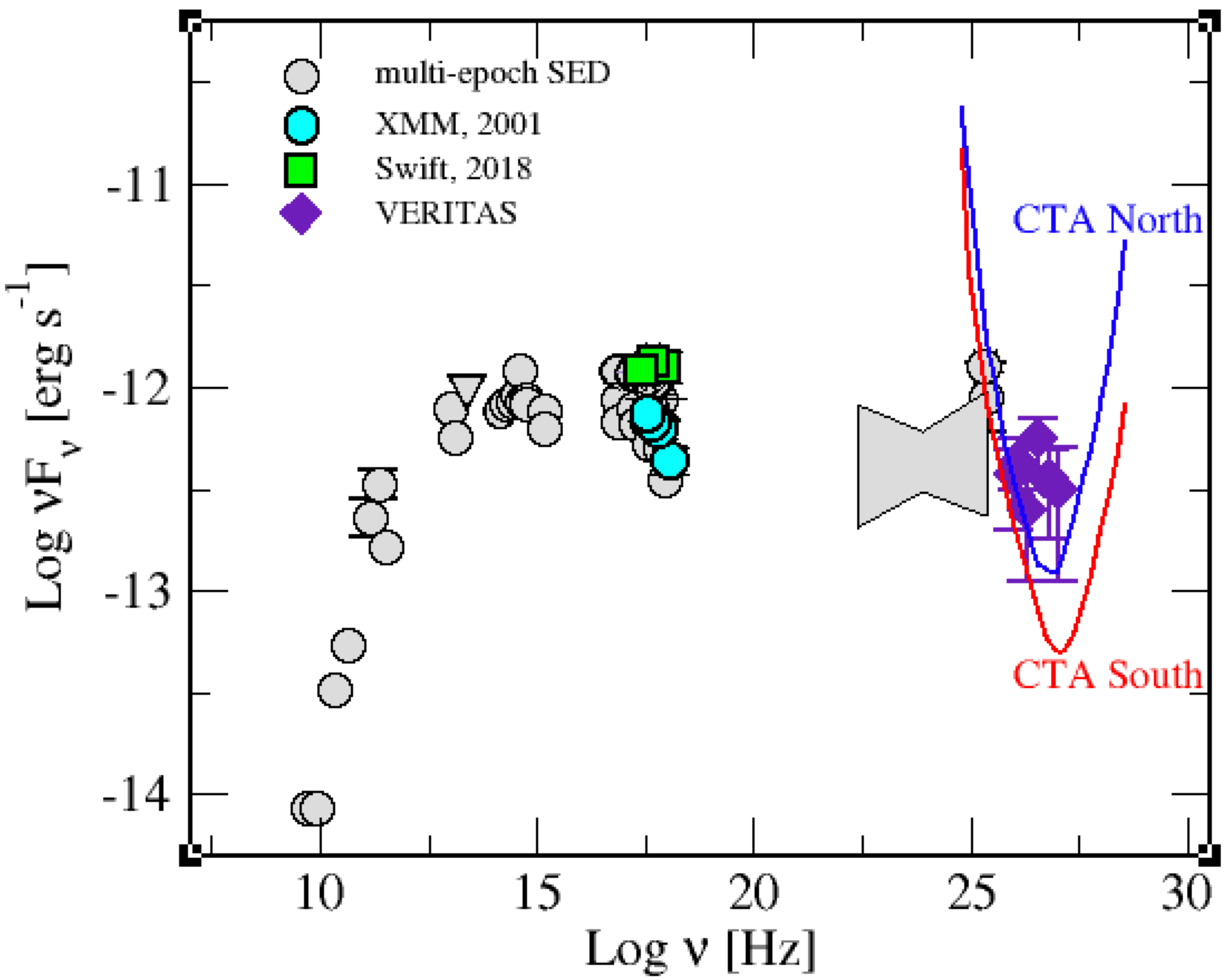

- CTA will improve the characterisation of the VHE emission (spectrum & variability) in radio galaxies;
- Need for coordinate mw-campaigns (radio, optical & X-rays).

	SLS		HHS		
Model Parameters	Core Model 1	Core Model 2&3	Core Model 1	Layer Model 2	Spine Model 3
Γ_{bulk}	2.0	2.0	2.0	5.0	8.0
θ	10.0	10.0	10.0	10.0	5.0
B (G)	0.055	0.12	0.062	0.0075	0.0035
B_{eq} (G)	0.09	0.04	0.15	0.03	0.023
R (cm)	6.5×10^{16}	3×10^{17}	2.3×10^{16}	1.15×10^{17}	7×10^{16}
γ_{min}	2×10^{3}	2×10^{2}	2×10^{3}	3×10^{3}	3×10^{3}
γ_{max}	1×10^{6}	4×10^{5}	3×10^{6}	2×10^{6}	2×10^{6}
γ_{break}	2×10^{4}	4×10^{3}	8.5×10^{4}	3.5×10^{3}	5×10^{3}
p_1	2.2	2.2	2.1	2.2	2.1
p_2	3.1	3.1	3.0	2.7	2.66
U_B/U_e	0.13	37.0	0.021	0.002	0.0003
Powers					
L_{rad} (erg s^{-1})	2.4×10^{41}	3.1×10^{41}	5.1×10^{41}	6.0×10^{41}	1.3×10^{41}
L_B (erg s^{-1})	1.7×10^{41}	1.7×10^{43}	2.6×10^{40}	6.8×10^{40}	1.4×10^{40}
L_e (erg s^{-1})	5.3×10^{41}	2.3×10^{41}	6.3×10^{41}	1.5×10^{43}	2.1×10^{43}
L_p (erg s^{-1})	1.6×10^{41}	6.3×10^{41}	1.4×10^{41}	3.9×10^{42}	5.0×10^{42}
L_{kin} (erg s^{-1})	7.0×10^{41}	8.6×10^{41}	7.7×10^{41}	1.9×10^{43}	2.6×10^{43}